Comparison of Four Automatic Detection Algorithm with Initial Parameters for DICOM Artificial Brain Shift

Kaoru Watanabe [1], Takumi Mori [1], Hiroshi Noborio [1,*], and Masanao Koeda [2]

[1] Osaka Electro-Communication University, Shijo-Nawate, Japan
[2] Okayama Prefectural University, Soja, Japan
Email: kaoru@osakac.ac.jp (K.W.); nobori@osakac.ac.jp (H.N.); koeda@ss.oka-pu.ac.jp (M.K.)
*Corresponding author

***Abstract*—In neurosurgery to remove brain tumors, DICOM data, a medical imaging standard, is generated preoperatively using CT and MRI. This data is used for surgical planning. However, brain deformities, known as brain shifts, can occur during surgery and deviate from the preoperative surgical plan. Deviations from the surgical plan due to brain shift are a life-threatening problem as they reduce the success rate of surgery. Brain shift has not yet been elucidated and DICOM data acquired by MRI and CT for surgical planning and post-operative management are stored and archived at hospitals and discarded after a certain period. To address these issues, we started research around 2018 with the goal of modelling brain shifts. This will enable surgical planning to take brain shifts into account during pre-operative conferences. The corresponding OpenCV feature points are extracted from the pre-operative and post-operative DICOM and the brain shift is extracted from their motion vectors. Here, the feature point extraction algorithms BRISK, AKAZE, ORB, and SIFT are compared and it is experimentally confirmed that BRISK and AKAZE have better brain shift extraction capability than the other two algorithms.**

***Keywords*—brain-shift, Digital Imaging and Communications in Medicine (DICOM), OpenCV's feature point**

I. Introduction

The brain is the most important organ in the human body and unnecessary damage during surgery must be avoided to prevent post-operative complications and sequelae. The brain must therefore be handled skillfully. In general, it is difficult to identify the boundary between normal and abnormal areas during surgery. For example, surgeons may overdo it when removing malignant tumors, reducing patient survival. Also, leaving too much of the malignant tumor may lead to recurrence.

Generally, before neurosurgery, Computed Tomography (CT) or Magnetic Resonance Imaging (MRI) is used to produce brain images of the patient using Digital Imaging and Communications in Medicine (DICOM) (two-dimensional top and bottom greyscale 124 images stacked vertically) are captured as DICOM images. These images are represented in a three-dimensional hierarchical structure of grey-valued voxels; using CT and MRI techniques, malignant tumors and aneurysms can be detected, along with blood vessels and nerves. During surgery, the neurosurgical navigation system shows the doctor the relationship between the site of the malignancy and the blood vessels and nerves. The relationship between the site of the malignancy and the blood vessels, as well as the position and posture of the scalpel, can be monitored in real time. The position and posture of the scalpel can be determined in real time.

However, as the brain is a soft organ, the brain itself is deformed during surgery, resulting in brain misalignment, where the image of the brain taken before surgery does not match the actual brain during surgery. Brain misalignment is a phenomenon in which the brain is deformed so that it sinks. Brain misalignment is a phenomenon in which the brain is deformed in such a way that it sinks. When spinal fluid is lost, the brain sinks towards the base of the skull. The brain sinks towards the base of the skull. In addition, when a malignant tumor or cerebral thrombus is removed, the surrounding tissue moves into the cavity. As a result, the position and morphology of the malignant tumor changes as follows. This is known as brain shift. From this brain shift, the position and morphology of the malignant tumor change during neurosurgery, reducing the accuracy of navigation guidance. Current neurosurgical navigation systems are unable to accurately predict and communicate this brain shift to the doctor. This can lead to surgical errors. This is the main concern of the co-principal investigators, neurosurgeons, in surgery.

Therefore, in this study, to build a model of the brain shift, the actual brain shift is extracted from a pair of preoperative and postoperative DICOMs; feature points extracted by OpenCV from the DICOMs are used as landmarks and the actual brain shift is extracted from their movements. To solve this problem, we aimed to develop a neurosurgical navigation system. The objective was to develop a neurosurgical navigation system. We aimed to create a brain model. Previous organ models

Manuscript received October 15, 2023; revised November 25, 2023; accepted March 12, 2024; published July 30, 2024.

doi: 10.18178/ijpmbs.13.3.74-79

were not backed by actual intraoperative data. Previous organ models were not backed by actual intraoperative data, and the plausibility of their deformations had not been evaluated [1–8]. Our goal was to create a brain model with deformations like intraoperative data. We aimed to create a brain model with deformations like intraoperative data by quantitatively detecting brain misalignments from pre- and postoperative brain DICOM images. In addition, we aimed to create a brain model with a deformation similar to that of intraoperative data by quantitatively detecting brain misalignment from pre- and postoperative brain DICOM images recorded at multiple hospitals. Therefore, over the past few years, we have developed a feature point detection algorithm [9–16] (e.g., AKAZE), an orientation feature From Accelerated Segment Test (FAST), a rotated Binary Robust Independent Feature (BRIEF), Oriented FAST and Rotated BRIEF (ORB), Binary Robust Invariant Scalable Key points (BRISK), Scale Invariant Feature Transform (SIFT), etc.) were used to extract a mapping set of similar feature points from the preoperative and postoperative DICOMs, which were employed as brain shifts. However, the correctness of this extracted brain shift could not be confirmed [17, 18].

Therefore, we developed an algorithm to artificially deform DICOM images locally [19]. Subsequently, as part of this study, we identified local brain misalignments detected by the feature point matching algorithm. Local brain misalignments detected by the feature point matching algorithm were identified. were identified. Based on this, the optimal feature point detection algorithm for detecting local brain shift was determined [20]. In this paper, we precisely check the best algorithm and its parameters for detecting an artificial brain-shift.

The structure of this paper is as follows. Section II provides an overview of our artificial brain shift algorithm for DICOM. Section III describes our brain shift detection algorithm for two DICOMs. Section IV describes experiments and evaluation. Section V presents conclusions.

II. Artificial Brain Shift Creation Algorithm for DICOM

To assess the correctness of the results of the brain shift detection algorithm, a method to artificially generate brain shifts was developed (Fig. 1). To support future brain shift modelling, Unity with its physics engine was used for development. Artificial brain shifts retain the coordinates of the deformation points before and after deformation, so it is possible to clearly identify which part of the brain has been deformed and to what extent. Therefore, the quality of the brain shift detection algorithm can be evaluated by comparing the results of the brain shift detection algorithm with the coordinates of the deformation points retained by the artificial brain shift. An advantage of our artificial brain shift generation method is that the deformation is feature point-based, so the feature points remain after the deformation. Since our brain shift detection system assumes that feature points remain after brain deformation, we develop an artificial brain shift system that is capable of feature point-based deformation. Here, we consider AKAZE, BRISK, ORB and SIFT as feature point detection algorithms.

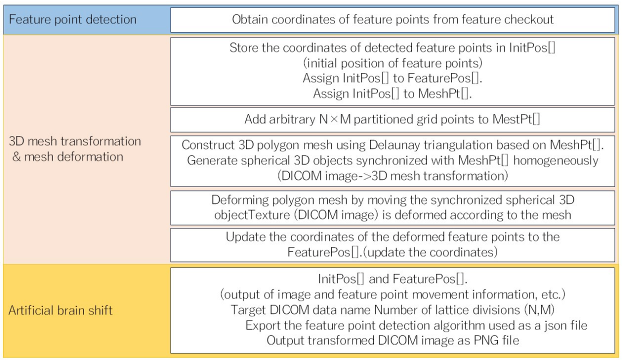

Feature point detection	Obtain coordinates of feature points from feature checkout
3D mesh transformation & mesh deformation	Store the coordinates of detected feature points in InitPos[] (initial position of feature points) Assign InitPos[] to FeaturePos[]. Assign InitPos[] to MeshPt[].
	Add arbitrary N×M partitioned grid points to MestPt[]
	Construct 3D polygon mesh using Delaunay triangulation based on MeshPt[]. Generate spherical 3D objects synchronized with MeshPt[] homogeneously (DICOM image->3D mesh transformation)
	Deforming polygon mesh by moving the synchronized spherical 3D objectTexture (DICOM image) is deformed according to the mesh
	Update the coordinates of the deformed feature points to the FeaturePos[].(update the coordinates)
Artificial brain shift	InitPos[] and FeaturePos[]. (output of image and feature point movement information, etc.) Target DICOM data name Number of lattice divisions (N,M) Export the feature point detection algorithm used as a json file Output transformed DICOM image as PNG file

Fig. 1. How artificial brain shift works.

To create an artificial brain shift, a feature inspection is first performed on the preoperative DICOM (Fig. 1). The feature point coordinates obtained from the feature point inspection are retained as the initial positions. The feature point coordinates are defined as x ($0 \le x \le M$), where x ($0 \le x \le M$) is the x-th abscissa of the grid point and y ($0 \le y \le N$) is the y-th ordinate of the grid point (Eqs. (1–3)). For compatibility with OpenCV and to facilitate calculation, the top-left edge is taken as the starting point (0, 0). However, in the Unity coordinate system, the y-axis becomes more negative towards the bottom. Therefore, the y-coordinate of the intersection point in Eqs. (1–3) is subtracted from the length of the preoperative DICOM image.

$$\text{Vertical length per lattice } Dh = \text{height}/N \tag{1}$$

$$\text{Horizontal length per lattice } Dw = \text{width}/M \tag{2}$$

$$\text{Coordinates } Pn \text{ of lattice points } (x\text{-}th,\ y\text{-}th) = (Dw \times \text{x},\ \text{-height} + Dh \times \text{y}) \tag{3}$$

Both feature points and grid points are operation points for deforming DICOM images. However, the edges of the DICOM image do not need to be deformed. Therefore, if x is the x-th abscissa of a grid point and y is the y-th ordinate of a grid point, no operation is accepted if x = 0, y = 0, x = M, and y = N.

After the coordinates of the grid points have been added, they are combined with the initial positions to form calculation points and construct a 3D polygon mesh. The polygon mesh is constructed using Delaunay triangulation. Delaunay triangulation produces a set of triangles with the calculation points as vertices (Fig. 2). The polygon mesh is constructed from these triangles.

Polygon meshes are created according to Unity's polygon mesh generation rules (mainly vertex coordinates, u_v coordinates, and the order of vertices forming a triangle); in Unity, each vertex is assigned a number 0, 1, or 2. A triangular polygon mesh is constructed by assigning each vertex a number 0, 1, or 2 and connecting the vertices in order from smallest to largest. The order in which the polygon mesh is generated determines whether it faces left or right, so the viewpoint and front-back relationship must be considered when generating the polygon mesh.

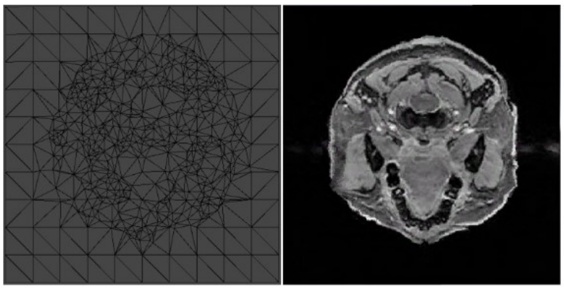

Fig. 2. Delaunay triangulation and polygon mesh being generated.

In Unity, vertex meshes cannot be manipulated directly in the GUI. Therefore, a separate object must be prepared as a GUI and synchronized with the vertex mesh by code. The object of the operation point is generated from the coordinates of the initial position of a combination of feature points and grid points. During the movement operation of this object, the coordinates of the operation points are synchronized with the coordinates of the vertex mesh to deform the mesh (Fig. 3). When deforming, the surrounding operation points are also deformed in conjunction. Therefore, it was considered burdensome to record and process the surrounding operation points for each individual operation point. Therefore, deformations were performed on all points so that the strength of each deformation decreases as the distance from the operation point, the center of the deformation, increases. As a result, the distant operation points were hardly deformed and the surrounding operation points were hardly deformed except at the surrounding operation points. When an operation point is deformed, all pixels in the mesh with the deformed operation point as the vertex mesh are deformed along the mesh, regardless of whether the deformation is a central deformation (around the operation point) or a connected deformation (around points away from the operation point). Let P be the operation point that performed the deformation operation, and let P be its vector and Q_n be the surrounding operation points, then the deformation vector of the surrounding operation points Q_n is as in Equation (4).

The magnitude of deformation of the surrounding operating point $f(n)$ = the magnitude of vector $P/\sqrt{}$(the distance between P and Q_n).

Deformation vector Q_n of surrounding operating points = the unit vector of $P \times f(n)$ (4)

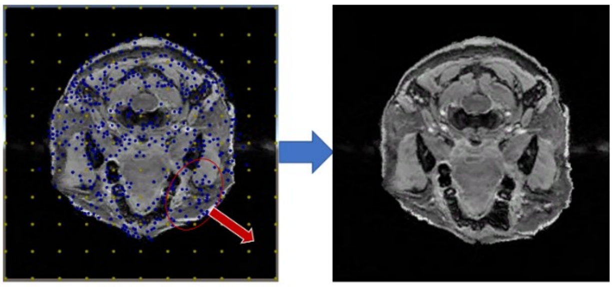

Fig. 3. Artificial brain shift generated by mesh deformation.

TABLE I. ALGORITHMS AND PARAMETERS EVALUATED

AKAZE	BRISK	ORB		SIFT
Detector threshold	AGAST detector threshold	FAST detector threshold		Threshold of the boundary meeting where no feature is detected
0.001	30	10	21	none
		10	31	
		10	41	
0.0005	20	20	21	
		20	31	
		20	41	
0.0001	10	30	21	
		30	31	
		30	41	

Feature point extraction is performed on the brain DICOM. To investigate how each algorithm varies with the threshold value, the threshold values are listed in Table I. To avoid unnatural deformations, the mesh was divided into a grid and the mesh granularity was increased. The number of divisions can be set arbitrarily, but in our experiments, we used three different artificial brain shifts: three different artificial brain shifts were used: 10×10, 20×20, and 30×30 respectively. Finally, a virtual DICOM with artificial brain shift was created by shifting arbitrary points. The number of feature points obtained from the real and virtual DICOMs was investigated. The results showed that the feature points obtained from BRISK and AKAZE were like those obtained from the brain DICOM. The distribution of feature points for both algorithms was uniform; BRISK and AKAZE were rated as more suitable than the other two algorithms. This is because the more feature points an artificial brain shift has, the greater the degree of freedom of deformation is.

III. BRAIN SHIFT DETECTION ALGORITHM FOR TWO DICOMS

Brain shift is detected by measuring the amount of movement of each feature point in the pre-operative and post-operative DICOM images by feature point matching. If the pre-operative feature points remain after surgery, the brain shift can be detected by measuring the amount of movement of the pre-operative feature points. The algorithm for detecting the brain shift is shown in Fig. 4.

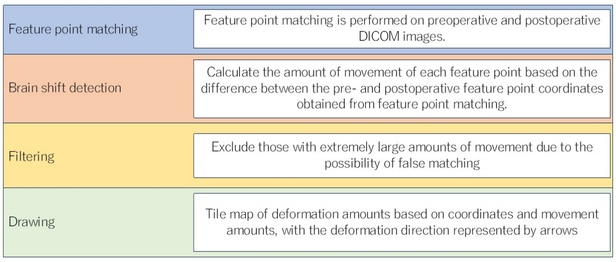

Feature point matching: Feature point matching is performed on preoperative and postoperative DICOM images.

Brain shift detection: Calculate the amount of movement of each feature point based on the difference between the pre- and postoperative feature point coordinates obtained from feature point matching.

Filtering: Exclude those with extremely large amounts of movement due to the possibility of false matching

Drawing: Tile map of deformation amounts based on coordinates and movement amounts, with the deformation direction represented by arrows

Fig. 4. How the brain shift detection algorithm works.

Brain shift is detected by measuring the amount of movement of each feature point in the preoperative and postoperative DICOM images by feature point matching. If the preoperative feature points remain after surgery, the brain shift can be detected by measuring the amount of movement of the preoperative feature points. The algorithm for brain shift detection is shown in Fig. 4.

This is an example of a point that should have been matched with P'_1 but was mistakenly matched with P'_n. The numbers above the points in Fig. 5 indicate the degree of similarity. The smaller the number, the higher the similarity and the more likely it is that they are at the same point. In this example, the similarity of the same point, P_1', is higher than the other points, but this is because the feature values have changed due to the deformation, indicating that another point was incorrectly matched. In this case, the extremely large displacement (length of the red arrow in Fig. 5) is an error and is not drawn.

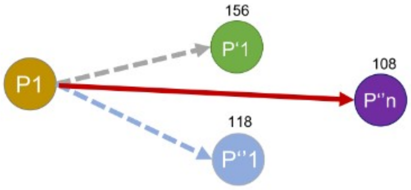

Fig. 5. Feature point matching error. P: Feature points obtained from preoperative DICOM; P': P moved by surgery (in postoperative DICOM); P'': feature point detected as P' by the feature point detection algorithm.

Rendering is expressed in the form of a color tile map, and the number of tile map divisions can be set to N for the vertical direction and M for the horizontal direction. Tile map rendering consists of three layers: the Draw layer, which writes color information on the amount of movement of the DICOM image; the Tile layer, which considers the influence of the surroundings when moving the image; and the Mono layer, which holds the amount of movement per px without considering the influence of the surroundings. In the draw layer, the preoperative draw layer matches the feature points of the preoperative and postoperative Dycom images and calculates the amount of movement of each site from the Euclidean distance between the preoperative and postoperative feature points. The amount of movement is stored in the Mono layer. In the tile layer, the height and width of each tile are calculated from the number of divisions N and M in the tile map. As tiles are rectangular, the range of each tile is calculated by calculating the coordinates of the four vertices. The influence on the surrounding tiles is then set based on the amount of movement between each feature point that a thing has. The influence is attenuated for each neighboring tile by an arbitrary factor with respect to its own movement. In this case, influence is set to decay by a factor of 0.5 for each tile moving away from the thing. However, as brain shifts become more apparent in the future, appropriate values will need to be set. As the colors should shift more from blue to red, the cyclic HSV color space is used to calculate the hue position from the shifts and effects to determine the rendered colors. Finally, based on the results of feature point matching, the direction of movement is calculated from the vector between the two feature points before and after surgery and an arrow is drawn (Figs. 6 and 7).

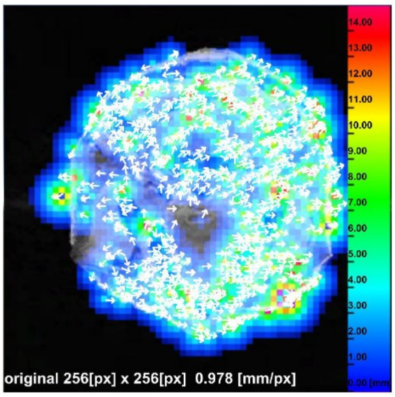

Fig. 6. Brain shift detection algorithm.

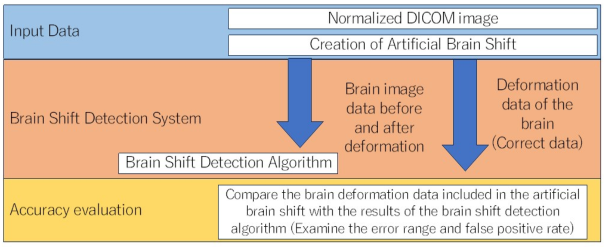

Input Data

Normalized DICOM image

Creation of Artificial Brain Shift

Brain Shift Detection System

Brain image data before and after deformation

Deformation data of the brain (Correct data)

Brain Shift Detection Algorithm

Accuracy evaluation

Compare the brain deformation data included in the artificial brain shift with the results of the brain shift detection algorithm (Examine the error range and false positive rate)

Fig. 7. Overall view of this study.

IV. Experiments and Evaluation

In this study, the following environment (OS Windows 10, CPU intel core i7 12700K, GPU RTX3080, Software used Unity 2021.3, Assets used OpenCVforUnity, DelaunayUnity) was used to search for the optimal feature point extraction algorithm was explored. In this section, each feature point detection algorithm is evaluated for a given set of initial parameters. First, the accuracy of the BRISK-derived artificial brain shift is evaluated using the accuracy evaluation method based on the maximum error and false positive rate of each feature point detection algorithm. The parameters are the initial values given in Table II and SIFT has no parameters.

TABLE II. Initial Parameter Values for Each Algorithm

Name	Default value for parameter 1	Default value for parameter 2
AKAZE	Detector threshold (0.0010000000474974)	–
BRISK	AGAST detector threshold (30)	–
ORB	FAST detector threshold (20)	Threshold of boundary at which no feature is detected (31)
SIFT	–	–

Table III shows the results of an experiment in which the parameters of each algorithm were given initial values for a single BRISK-derived artificial brain shift. The maximum error for each algorithm is large, especially for ORB.

TABLE III. ACCURACY EVALUATION OF EACH ALGORITHM WHEN GIVEN INITIAL VALUE PARAMETERS

Name	Maximum error (mm)	False positive rate (%)
AKAZE	21	0
BRISK	17	0
ORB	42	0
SIFT	22	–

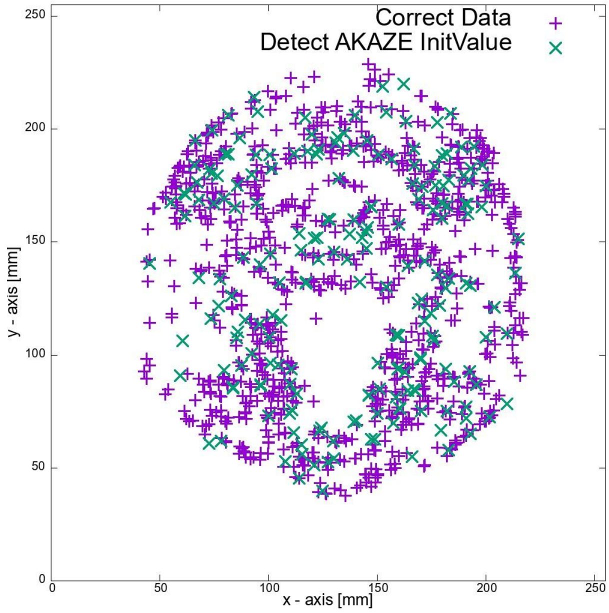

Fig. 8. Overlap with the answer when the AKAZE detector is given an initial value.

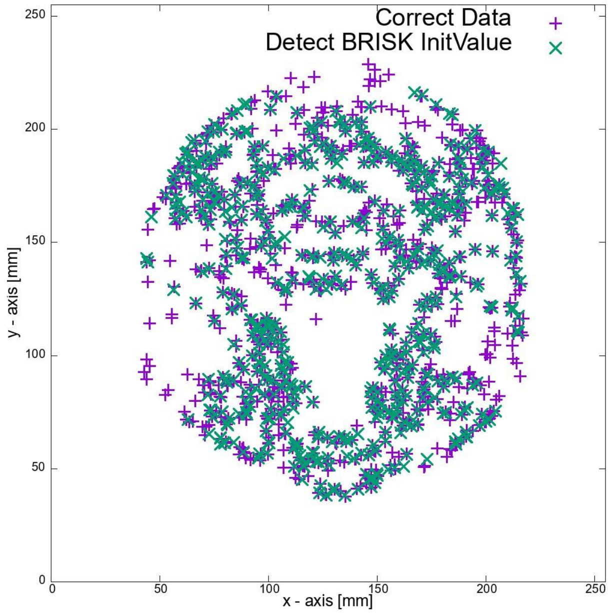

Fig. 9. Overlap with the answer when initial values are given to the AGAST detector in BRISK.

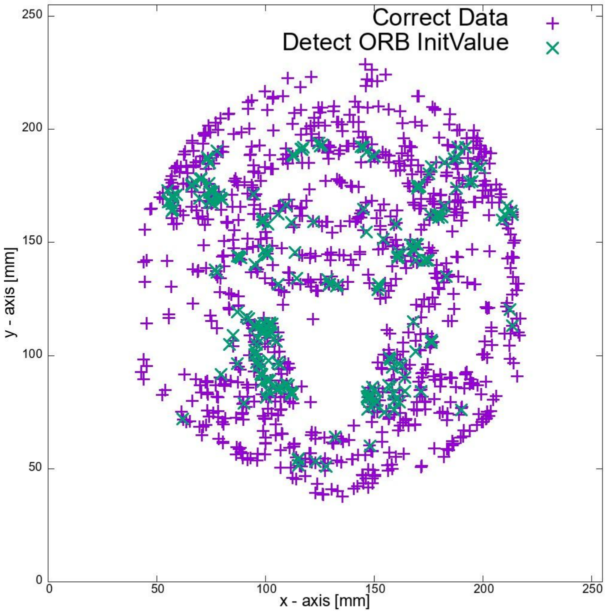

Fig. 10. Overlap with the answer when the ORB is given an initial value.

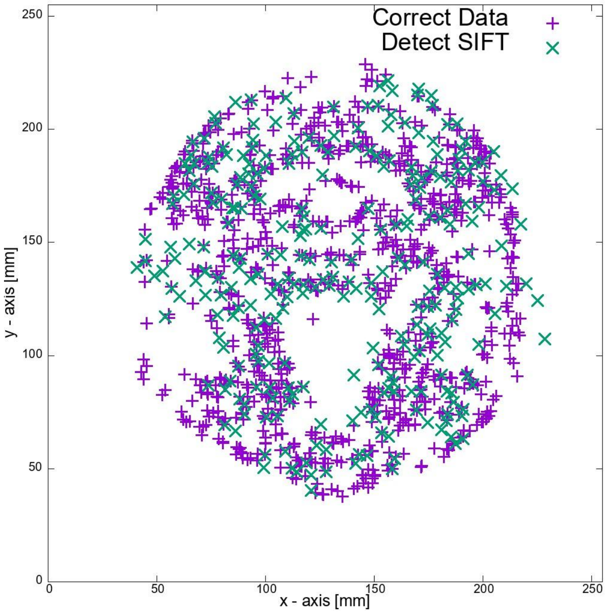

Fig. 11. Overlap with SIFT answers.

Figs. 8–11 show these results in feature point coordinates. The overlap between x detected by the feature point detection algorithm and the post-operative feature point + retained by the artificial brain shift is shown for each of the four algorithms: the greater the overlap between x and x, the more deformations have been tracked and detected. In other words, the better the feature point detection algorithm, the more purple + (post-operative feature point +) is lost. The results in Figs. 8–11 show that BRISK is the best, ORB is the worst, and SIFT and AKAZE are in between. However, this is a result and SIFT has no adjustment parameters, whereas AKAZE has adjustment parameters and can still be adjusted.

V. Conclusions

In the accuracy assessment of each algorithm, BRISK had the smallest maximum error given the initial parameters. This was because the feature detections were evenly distributed throughout the brain. On the other hand, ORB had an uneven distribution of feature detection and failed to detect deformations in some parts of the brain. These results may have affected the maximum error, and the maximum error of AKAZE was like that of SIFT. However, SIFT cannot accurately detect brain deformations because it has no parameters. AKAZE, on the other hand, can change its results in the future by adjusting the parameters.

Conflict of Interest

The authors declare no conflict of interest.

Author Contributions

Kaoru Watanabe, Hiroshi Noborio, and Masanao Koeda contributed to the research concept and design, and conceived the project and the study hypothesis; Kaoru Watanabe designed the algorithm with programming, and Takumi Mori and Masanao Koeda designed the software, respectively; Hiroshi Noborio and Masanao Koeda analyzed the data executed from them, and checked the data; Kaoru Watanabe analyzed and evaluated the data; Hiroshi Noborio wrote the paper by manuscript rewriting; all authors have approved the final version.

Funding

This study was partly supported by 2017 and 2020 Grants-in-Aid for Scientific Research (C) (No. 17K00420 and 20K12053) from the Ministry of Education, Culture, Sports, Science, and Technology, Japan. Further support was provided by the 2022 Cooperation Research Fund B from the Graduate School at Osaka Electro-Communication University.

References

[1] K. Sun, T. S. Pheiffer, A. L. Simpson, J. A. Weis, R. C. Thompson, and M. I. Miga, "Near real-time computer assisted surgery for brain shift correction using biomechanical models," *IEEE Journal of Translational Engineering in Health and Medicine*, vol. 2, pp. 1–13, 2014.

[2] I. Chen, R. E. Ong, A. L. Simpson, K. Sun, R. C. Thompson, and M. I. Miga, "Integrating retraction modeling into an atlas-based framework for brain shift prediction," *IEEE Transactions on Biomedical Engineering*, vol. 60, no. 12, pp. 3494–3504, 2013.

[3] C. DeLorenzo, X. Papademetris, L. H. Staib, K. P. Vives, D. D. Spencer, and J. S. Duncan, "Volumetric intraoperative brain deformation compensation: Model development and phan-tom validation," *IEEE Transactions on Medical Imaging*, vol. 31, no. 8, pp. 1607–1619, 2012.

[4] L. M. Vigneron, R. C. Boman, J.-P. Ponthot, P. A. Robe, S. K. Warfield, and J. G. Verly, "Enhanced FEM-based modeling of brain shift deformation in image-guided neurosurgery," *Journal of Computational and Applied Mathematics*, vol. 234, no. 7, pp. 2046–2053, 2010.

[5] E. I. Zacharaki, C. S. Hogea, G. Biros, and C. Davatzikos, "A comparative study of biome-chanical simulators in deformable registration of brain tumor images," *IEEE Transactions on Biomedical Engineering*, vol. 55, no. 3, pp. 1233–1236, 2008.

[6] Y. Payan, *Soft Tissue Biomechanical Modeling for Computer Assisted Surgery. Part of the Studies in Mechanobiology. Tissue Engineering and Biomaterials Book Series*, New York: Springer, 2012, vol. 11.

[7] A. Valencia, B. Blas, and J. H. Ortega, "Modeling of brain shift phenomenon for different craniotomies and solid models," *Journal of Applied Mathematics*, vol. 2012, no. 12, article ID 409127, February 2012.

[8] D. G. Lowe, "Distinctive image features from scale-invariant keypoints," *Int. Journal of Computer Vision*, vol. 60, no. 2. pp. 91–110, 2004.

[9] M. Hassaballah, *et al.*, "Image features detection description and matching," in *Image Feature Detectors and Descriptors*, Springer International Publishing, 2016, pp. 11–45.

[10] K. Mikolajczyk and C. Schmid, "A performance evaluation of local descriptors," *IEEE Transactions on Pattern Analysis and Machine Intelligence*, vol. 27, no. 10, pp. 1615–1630, 2005.

[11] P. F. Alcantarilla, *et al.*, "KAZE features," in *Proc. European Conference on Computer Vision*, 2012, pp. 214–227.

[12] P. F Alcantarilla, J. Nuevo, and A. Bartoli, "Fast explicit diffusion for accelerated features in nonlinear scale spaces," *Trans. Pattern Anal. Machine Intell.*, vol. 34, no. 7, pp. 1281–1298, 2011.

[13] E. Rublee, *et al.*, "ORB: An efficient alternative to SIFT or SURF," in *Proc. IEEE International Conference on Computer Vision*, 2011, pp. 2564–2571.

[14] E. Rosten and T. Drummond, "Machine learning for high-speed corner detection," in *Proc. European Conference on Computer Vision*, 2006, pp. 430–443.

[15] M. Calonder, *et al.*, "Brief: Binary robust independent elementary features," in *Proc. European Conference on Computer Vision*, 2010, pp. 778–792.

[16] S. Leutenegger, *et al.*, "BRISK: Binary robust invariant scalable keypoints," in *Proc. IEEE International Conference on Computer Vision*, 2011, pp. 2548–2555.

[17] H. Noborio, S. Uchibori, M. Koeda, and K. Watanabe, "Two-dimensional DICOM feature points and their mapping extraction for identifying brain shifts," *International Journal of Pharma Medicine and Biological Sciences*, vol. 8, no. 3, pp. 71–78, July 2019.

[18] H. Noborio, S. Uchibori, M. Koeda, and K. Watanabe, "Visualizing the correspondence of feature point mapping between DICOM images before and after surgery," in *Proc. the 2019 11th International Conference on Bioinformatics and Biomedical Technology*, Stockholm, Sweden, May 29–31, 2019, pp. 1–7.

[19] T. Mori, M. Nonaka, T. Kunii, M. Koeda, and H. Noborio, "Development of an algorithm to artificially create virtual brain deformations for brain DICOM," in *Human-Computer Interaction. Interaction Techniques and Novel Applications*, M. Kurosu, Ed., Springer, 2022, pp. 388–402.

[20] T. Mori, M. Nonaka, T. Kunii, M. Koeda, K. Watanabe, and H. Noborio, "Algorithm for automatic brain-shift detection using the distance between feature descriptors," in *Human-Computer Interaction. Interaction Techniques and Novel Applications*. M. Kurosu, Ed., Springer, 2022, pp. 376–387.

Copyright © 2024 by the authors. This is an open access article distributed under the Creative Commons Attribution License (CC BY-NC-ND 4.0), which permits use, distribution and reproduction in any medium, provided that the article is properly cited, the use is non-commercial and no modifications or adaptations are made.